2010 IEEE International Conference on Robotics and Automation
Anchorage Convention District
May 3-8, 2010, Anchorage, Alaska, USA

Stable and Robust Walking with Compliant Legs

Juergen Rummel, Yvonne Blum, H. Moritz Maus, Christian Rode and Andre Seyfarth

Abstract— **Bipedal walking could be implemented into a robot by mimicking spring-like leg behaviour. The fundamental model, describing human-like leg function in walking is the bipedal spring-mass model which was investigated in this study. We identified several types of walking patterns, e.g. symmetric and asymmetric walking, that accounts for high variability of gait. The aim of this study is the identification of a stiffness range which allows for stable walking with comparatively large robustness against perturbations. Walking with compliant legs was tested with the bipedal PogoWalker, demonstrating advantages of the underlying leg mechanics, i.e. walking without the necessity of precise leg adjustments, and acceptable impact forces.**

I. Introduction

The most common gait of humans is walking on two legs. Whereas human walking seems to be naturally internalized, it appears to be complicated to implement bipedal gaits into artificial systems (e.g. walking robots, prostheses). A class of artificial bipeds emulating human-like walking are the passive dynamic walkers, having straight legs during stance phase [1]. The straight leg mechanism provides a remarkable energy efficiency in locomotion but minor robustness against perturbations [2]. In contrast, human legs are never completely straight in walking, although the body is clearly lifted during midstance [3]. Investigations on leg dynamics revealed a spring-like leg mechanism. This was demonstrated with the bipedal spring-mass model, providing patterns of ground reaction forces similar to those found in human walking [4]. A key requirement for successful walking is stability, which is also predicted by the bipedal spring-mass model. Another important feature of spring-like leg mechanics is the reduction of impact forces, preventing the system from damage. Leg compliance not necessarily has to be generated by physical springs. It could also be actively simulated as it was demonstrated in a robot hopping vertically [5].

While compliant leg mechanisms have already been implemented in walking robots [6], [7], [8], [9], performance and limitations of spring-like legs in walking are still rather unknown. The first purpose of this study is to analyze the capabilities of spring-like legs to generate walking patterns, represented by the size and structure of the parameter space and the range of possible walking speeds. As the periodicity of gait establishes a basis for stabilizing swing-leg strategies [10], we begin with the investigation of periodic walking patterns. In order to identify periodic gaits we introduce a Poincaré section at the instant of Vertical Leg Orientation (VLO) during single support (Fig. 1), that allows for the investigation of both, walking and running, with the same method. Here, we focus on human-like walking characterized by double support phases and two humps in the vertical ground reaction force.

J. Rummel, Y. Blum, H. M. Maus and A. Seyfarth are with the Lauflabor Locomotion Laboratory, University of Jena, Dornburger Straße 23, D-07743 Jena, Germany juergen.rummel@uni-jena.de

C. Rode is with the Institute of Motion Science, University of Jena, Seidelstraße 20, D-07749 Jena, Germany

This study was supported by an Emmy-Noether grant of the German Research Foundation (DFG) to A. Seyfarth (SE1042/1 and SE1042/7).

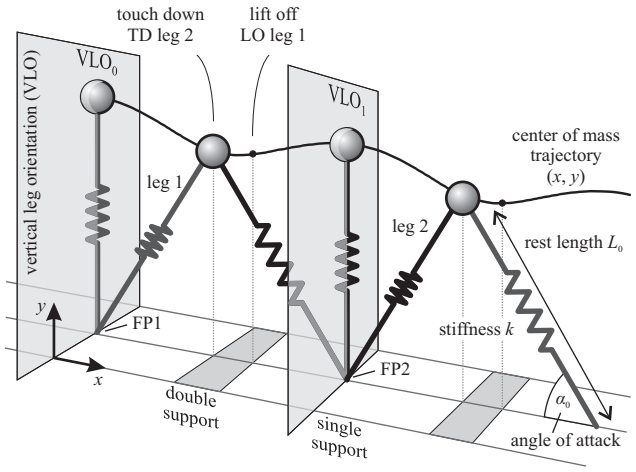

Fig. 1. The bipedal spring-mass model for walking. The simulation starts at the instant of vertical leg orientation (VLO) during single support phase and one step is completed at VLO of the counter leg.

To guarantee stable walking with compliant legs, leg stiffness is a crucial parameter in the robot design. Here, we ask which stiffness value would be a good choice for bipedal systems. Therefore, the second purpose of this study is to identify a leg stiffness that provides stable and robust walking.

While this paper is focusing on a simulation study, we also present data of preliminary walking experiments on a bipedal robot with compliant telescoping legs (PogoWalker) and compare them with the bipedal spring-mass model.

II. Methods

For investigating walking the bipedal spring-mass model [4] is used (Fig. 1). It describes the action of the spring-like stance legs supporting the body (represented as a point mass m) against gravity. The legs are massless telescopic springs of stiffness k and rest length L_0. During ground contact for leg 1, it exerts a force $\boldsymbol{F_1}$ on the point mass directed from the foot point $\boldsymbol{r}_{\mathbf{FP1}}$ to the center of mass $\boldsymbol{r} = [x, y]^{\mathrm{T}}$. During swing phase, the force $\boldsymbol{F_1}$ is zero and the leg has no influence on system dynamics.

The bipedal spring-mass model is acting in the sagittal plane. The equation of motion is

$$m\ddot{\boldsymbol{r}} = \boldsymbol{F_1} + \boldsymbol{F_2} - m\,\boldsymbol{g} \tag{1}$$

where $\boldsymbol{g} = [0, g]^{\mathrm{T}}$ is the gravitational acceleration with $g = 9.81\,\mathrm{m\,s^{-2}}$. The force of leg 1 during stance is defined as

$$\boldsymbol{F_1} = k\left(\frac{L_0}{|\boldsymbol{r} - \boldsymbol{r}_{\mathrm{FP1}}|} - 1\right)(\boldsymbol{r} - \boldsymbol{r}_{\mathrm{FP1}})\,. \tag{2}$$

When the force decreases to zero the leg's state changes from stance to swing phase. The transition from swing to stance occurs when the landing condition $y_{\mathrm{TD}} = L_0\,\sin(\alpha_0)$ is fulfilled while the vertical velocity $\dot{y}$ is negative. The parameter α_0 is the constant angle of attack.

The bipedal spring-mass model has a total number of five system parameters: body mass m, leg length L_0, stiffness k, angle of attack α_0, and the total system energy E. In order to compare the model with other legged systems of different size, dimensional analysis can be applied. Herewith, the number of parameters can be reduced to three fundamental parameters [4], i.e. the dimensionless leg stiffness $\widetilde{k} = k\,L_0/(m\,g)$, the angle of attack α_0, and the dimensionless system energy $\widetilde{E} = E/(L_0\,m\,g)$. In the simulations presented here the individual parameters are based on human dimensions, i.e. body mass $m = 80\,\mathrm{kg}$ and leg length $L_0 = 1\,\mathrm{m}$.

The bipedal spring-mass model is capable of periodically repeated gait patterns like walking and running. A gait pattern is fully described by the system parameters and the initial conditions $\boldsymbol{r_0} = [x_0, y_0]^{\mathrm{T}}$, and $\dot{\boldsymbol{r}}_{\boldsymbol{0}} = [\dot{x}_0, \dot{y}_0]^{\mathrm{T}}$. The initial conditions are chosen such that one leg has ground contact and is orientated vertically ($x = x_{\mathrm{FP1}}$). This event is called Vertical Leg Orientation (VLO). A single step is completed when the second leg has ground contact and the hip respectively the center of mass is perpendicular to the foot point ($x = x_{\mathrm{FP2}}$). With these definitions, the number of independent initial conditions can be reduced. At the instant of VLO the horizontal position is zero with respect to the actual foot point. Due to energy conservation of the model, the initial velocity's magnitude $|\dot{\boldsymbol{r}}_{\boldsymbol{0}}|$ depends on system parameters and on the initial height y_0:

$$|\dot{\boldsymbol{r}}_{\boldsymbol{0}}|^2 = \frac{2}{m}\left(E - m\,g\,y_0 - \frac{k}{2}\,(L_0 - y_0)^2\right). \tag{3}$$

The direction of motion can be represented by the velocity angle $\theta_0 = \arctan(\dot{y}_0/\dot{x}_0)$ and therefore, the velocity components $\dot{x}_0$ and $\dot{y}_0$ can be expressed using trigonometric relations. Hence, the two independent initial conditions are the height y_0 and the velocity angle θ_0 at VLO.

A legged system can be investigated by analyses of single-step Poincaré maps of the state vector $\boldsymbol{S}$ with VLO as Poincaré section. The mapping function is $\boldsymbol{S_{i+1}} = \boldsymbol{F}(\boldsymbol{S_i})$ where i is the number of the individual step. $\boldsymbol{S_i}$ denotes the system's state at the instant of VLO with $\boldsymbol{S_i} = [y_i, \theta_i]^{\mathrm{T}}$. A periodic gait pattern (limit-cycle trajectory) corresponds to a fixed point in the Poincaré map $\boldsymbol{S^*} = \boldsymbol{F}(\boldsymbol{S^*})$. Stability of a periodic solution is estimated by calculating the effect of small perturbations in the neighborhood of the fixed point. Therefore, a linear approximation is applied $[\boldsymbol{S_{i+1}} - \boldsymbol{S^*}] = \boldsymbol{J}(\boldsymbol{S^*})\,[\boldsymbol{S_i} - \boldsymbol{S^*}]$ where $\boldsymbol{J}(\boldsymbol{S^*})$ is the Jacobian matrix, with its eigenvalues λ_j called Floquet multipliers. Dynamic stability of the periodic gait is indicated if the magnitude of all eigenvalues is smaller than one [11].

If stability of a periodic gait pattern is identified, a corresponding basin of attraction within the state space exists. For calculating the boundary of the basin of attraction two methods were applied. The first method requires an additional fixed point, namely a saddle-node which is characterized by having one eigenvalue $|\lambda_1|$ greater than one and the other $|\lambda_2|$ less than one. The boundary of the basin of attraction is defined by the stable manifold of this saddle node [11], [12] which can be calculated by iterating this manifold backwards in time.

If there exists no saddle-node or the stable manifold cannot be calculated completely, an intuitive steps-to-fall method is applied for estimating the basin. Here, the number of steps is calculated for every rasterized combination of initial conditions. If the trial was successful, i.e. a minimum number of 50 walking steps was reached, and the system's state variables converge towards the stable fixed point, the initial conditions are located within the basin of attraction. The boundary of the basin of attraction is estimated with a higher precision by refining the underlying grid. The area of the enclosed basin of attraction characterizes the amount of robustness of the stable gait pattern.

The model is implemented in MATLAB/SIMULINK (R2007b, The MathWorks Inc., Natick, MA, USA) using a Runge-Kutta variable step integrator (ode45) with absolute and relative error tolerance of 10^{-11}. Periodic gait patterns were computed using a Newton-Raphson algorithm and a pattern is identified when the deviation between initial conditions and state space after one step $\sum_{j=1}^{2} |S_{i+1,j} - S_{i,j}|$ is less than 10^{-9}.

III. RESULTS

The bipedal spring-mass model reveals several kinds of periodic walking patterns which can be characterized by the number of peaks in the shape of the ground reaction force. In this paper we focus on human-like walking, where two peaks can be observed in the normal walking patterns. First, we describe such periodic walking patterns based on a fixed representative leg stiffness of $\widetilde{k} = 20$ identical to PogoWalker's leg stiffness (section IV).

Fig. 2 shows the independent initial conditions of periodic walking solutions for given angles of attack and selected system energies. There exist symmetric walking patterns (e.g. A and B) shown in Fig. 2(a) with zero velocity angle θ_0. Here, the center of mass trajectory is mirror-symmetric about midstance [13] and the instant of VLO equals midstance. Asymmetric walking patterns are shown in Fig. 2(b) with the corresponding velocity angle in Fig. 2(c). Whereas each single step is equal to the previous step, in asymmetric patterns the center of mass trajectory cannot be mirrored through VLO or other events (patterns C and D in Fig. 3).

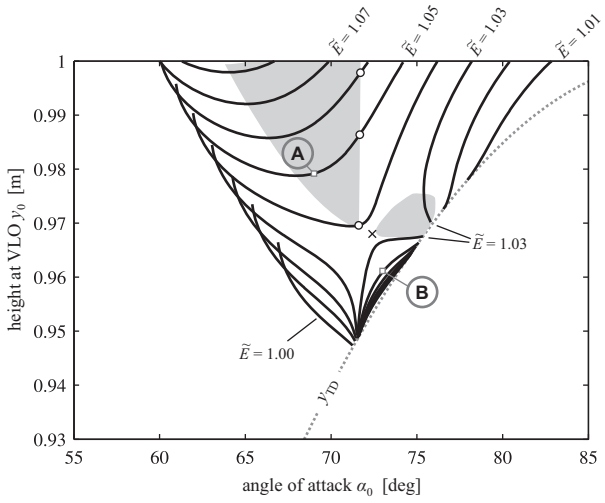

(a)

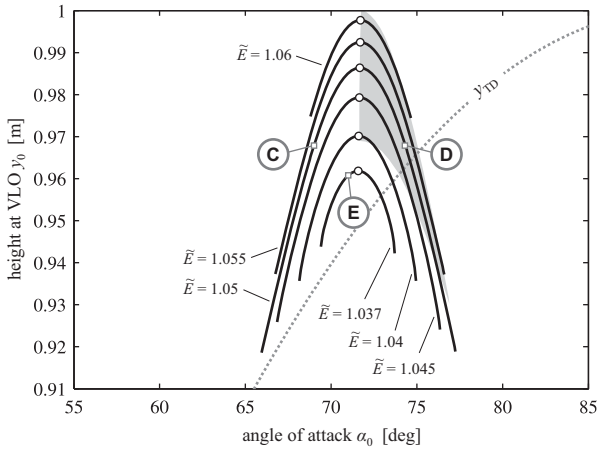

(b)

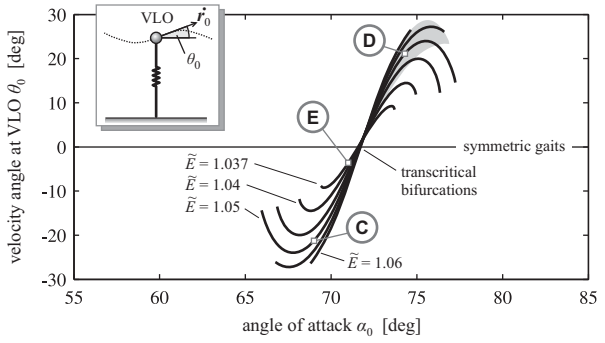

(c)

Fig. 2. Initial conditions (y_0, θ_0) with respect to angle of attack α_0 of (a) symmetric ($\theta_0 = 0$), and (b) and (c) asymmetric walking patterns for selected dimensionless system energies $\widetilde{E}$ and one leg stiffness $\widetilde{k} = 20$. Each point represents a periodic walking solution and the circles indicate transcritical bifurcations where asymmetric patterns cross the symmetric ones. The cross in (a) indicates a two-parameter bifurcation. Gray shaded areas represent regions of stable walking solutions. The dotted line is the touch down height $y_{\mathrm{TD}}(\alpha_0)$. The examples A-E are shown in Fig. 3.

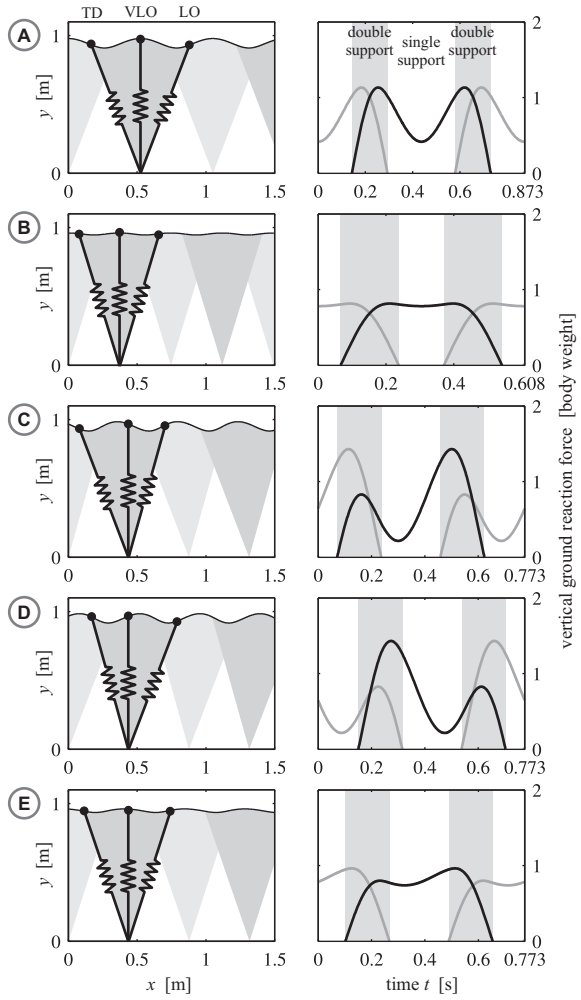

Fig. 3. Stick figures (left) of representative walking patterns related to the selections in Fig. 2. The emphasized events in the left column are touch down (TD), the instant of vertical leg orientation (VLO), and lift off (LO) of the second leg. The right column shows normalized ground reaction forces of a complete gait cycle.

Asymmetric patterns exist for both, positive and negative velocity angles, and transcritical bifurcations (i.e. intersections with symmetric walking patterns) arise (circles in Fig. 2(a) and 2(b)). The asymmetric walking patterns are point symmetric regarding the transcritical bifurcation. Pattern C and D are selected to show this feature. The lift off angle in C is equal to the angle of attack in D, and vice versa.

In general, for a given system energy the average velocity decreases with increasing angle of attack. For example, the velocity of pattern A ($\alpha_0 = 69\,\mathrm{deg}$, $\widetilde{E} = 1.05$) decreases from $1.20\,\mathrm{m/s}$ to $1.07\,\mathrm{m/s}$ for $\alpha_0 = 73\,\mathrm{deg}$ and constant energy. In the majority of cases, for a given angle of attack the height at VLO increases with increasing system energy. This indicates that the system transfers comparatively much of the additional energy into potential energy, i.e. the center of mass bounces more. Therefore, for a given angle of attack the average velocity increases slightly due to the added energy. For example, at pattern A (see above) the average velocity increases from $1.20\,\mathrm{m/s}$ to $1.24\,\mathrm{m/s}$ when system energy increases about $\Delta\widetilde{E} = 0.02$. A total transfer into kinetic energy would imply a velocity gain of $0.63\,\mathrm{m/s}$. In

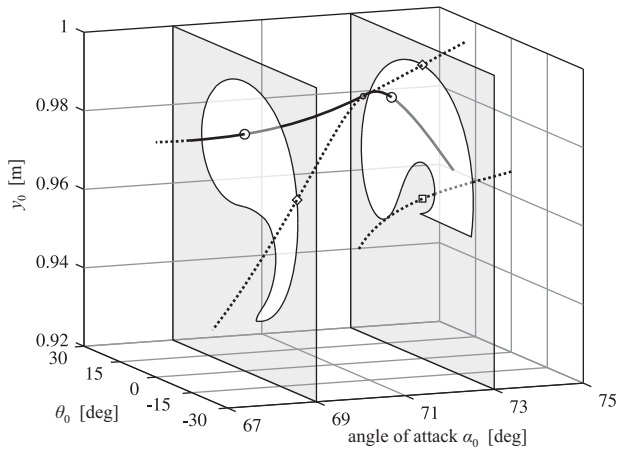

Fig. 4. Stable (thick solid lines) and unstable (dotted lines) fixed points in the VLO return map and two examples of the basin of attraction (white transparent areas) that are spanned in the state space (VLO height y_0, and velocity angle θ_0). The circle ∘ represents the stable fixed point and the diamond ⋄ indicates the saddle node required for calculating the boundary of the basin of attraction. The constant parameters are $\widetilde{k} = 20$, and $\widetilde{E} = 1.05$.

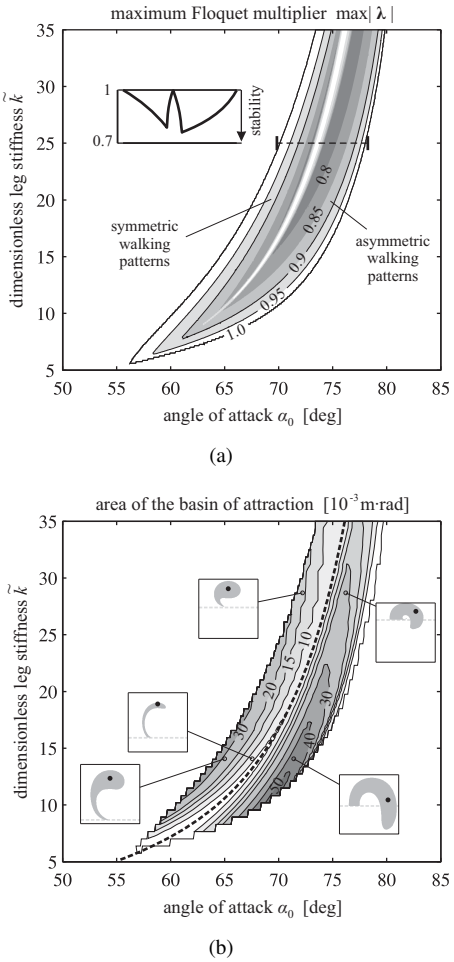

Fig. 5. Stability and robustness of stable walking solutions. The maximum Floquet multiplier in (a) illustrates compensation of small perturbations while $\max|\lambda| = 0$ would indicate dead-beat behavior. A detailed example is displayed for $\widetilde{k} = 25$. The area of the basin of attraction in (b) is an estimation for robustness to larger perturbations. It was calculated with a coarser grid due to the enormous computational effort. The dashed line in (b) indicates transcritical bifurcations separating stable symmetric and asymmetric walking. System energy depends on leg stiffness using equation 4. The icons in (b) show examples of basins of attraction with the stable fixed point (black dots), and the touch down heights y_{TD} (horizontal lines) within the ranges $\theta_0 = [-40,\ 40]\,\mathrm{deg}$, and $y_0 = [0.9,\ 1]\,\mathrm{m}$.

contrast, the walking solutions pattern B belongs to, constitute an exception: Here, with increasing energy the vertical oscillation of the bipedal spring-mass model decreases and more energy is transfered into kinetic energy. For example, the average velocity of pattern B ($\alpha_0 = 73\,\mathrm{deg}$, $\widetilde{E} = 1.05$) increases from $1.23\,\mathrm{m/s}$ to $1.38\,\mathrm{m/s}$ by increasing system energy about $\Delta\widetilde{E} = 0.02$. The walking solutions were calculated for a maximum energy of $\widetilde{E} = 2.5$, where a speed of $5.47\,\mathrm{m/s}$ was found for a walking pattern similar to pattern B. Minimum and maximum average velocity for patterns of type A are $0.10\,\mathrm{m/s}$ ($\widetilde{E} = 1.00$, $\alpha_0 = 88.3\,\mathrm{deg}$) and $1.41\,\mathrm{m/s}$ ($\widetilde{E} = 1.083$, $\alpha_0 = 62.2\,\mathrm{deg}$), respectively.

In cases of pattern B, we observe a morphing from two-peak ground reaction forces (Fig. 3) to single-peak forces when energy is increased or when the angle of attack gets flatter. However, these patterns require a very short time for swinging the leg forward, e.g. $0.13\,\mathrm{s}$ in pattern B.

The symmetric walking solutions belonging to pattern B are disconnected from those of other patterns by a bifurcation at $\widetilde{E} = 1.0392$ and $\alpha_0 = 72.4\,\mathrm{deg}$ in a two-parameter space ($\widetilde{E}$, α_0) shown as a cross in Fig. 2(a). This bifurcation is not related to the previously mentioned transcritical bifurcations where asymmetric solutions intersect symmetric ones which occur at $\alpha_0 \approx 71.6\,\mathrm{deg}$.

Stability is an important aspect for legged locomotion. The bipedal spring-mass model shows self-stable walking patterns as indicated by the gray areas in Fig 2. For energies $\widetilde{E} > 1.0392$ there exist two parameter regions of self-stable walking solutions. The first stable region contains symmetric walking patterns and is limited on the left side by the minimum VLO heights and on the right side by the transcritical bifurcations (Fig. 2(a)). The second region contains asymmetric walking patterns and starts at the mentioned transcritical bifurcations. Another small region of self-stable symmetric walking patterns is identified for energies smaller than $\widetilde{E} = 1.0392$. All walking solutions related to pattern B are unstable, indicated by maximum Floquet multipliers larger than one. To give an example, at a speed of $2\,\mathrm{m/s}$ the best respectively lowest value of maximum Floquet multipliers is $\max|\lambda| = 10.2$. Moreover, with increasing speed the maximum Floquet multipliers rise too.

So far, the description of walking gaits was done for a constant leg stiffness. Within the explored range of stiffness $\widetilde{k} = [5,\ 35]$, the general structure shown in Fig. 2 does not change. However, the distribution in angle of attack of periodic walking solutions decreases with increasing leg stiffness. Symmetric walking patterns exist in the range of $\alpha_0 = [38.0,\ 85.7]$ and $[65.0,\ 86.8]$ for a stiffness of $\widetilde{k} = 6$ and 30, respectively. Furthermore, there is a shift in system energy which can be explained using asymmetric

walking patterns. For example, asymmetric walking is found in the range of $\widetilde{E} = [0.954, 1.041]$ and $[1.047, 1.065]$ for a stiffness of $\widetilde{k} = 6$ and 30, respectively. The energy range decreases with increasing leg stiffness. Due to the fact that there is no overlap in energy between low and high stiffness, a comparison with a constant system energy would not make sense. Therefore, the comparison was done by taking the energy shift into account. For each leg stiffness a representative energy, i.e. the energy where the α_0-range of asymmetric patterns is maximal, was chosen. This energy can be best approximated with

$$\widetilde{E}(\widetilde{k}) = -0.054\ \log_{10}(\widetilde{k})^2 + 0.189\ \log_{10}(\widetilde{k}) + 0.898. \quad (4)$$

Self-stable walking can be found for leg stiffness higher than $\widetilde{k} = 5.5$ as shown in Fig. 5(a). The α_0-range of stable solutions increases with increasing stiffness until $\widetilde{k} = 15$ and then slightly decreases.

As a criterion for selecting system parameters, more important than stability, is the robustness of already stable walking solutions. For this purpose, the area of the basin of attraction was calculated, exemplarily illustrated for two selected walking patterns in Fig. 4. The basin of attraction at $\alpha_0 = 69\,\mathrm{deg}$ is completely enclosed by the stable manifolds of the saddle node. In the second example ($\alpha_0 = 73\,\mathrm{deg}$) the basin of attraction is limited by the touch down height $y_0 = y_{\mathrm{TD}}$ for negative velocity angles θ_0. Below this limit further steps are impossible because the touch down condition cannot be fulfilled. Here, the boundary of the basin of attraction was determined by a combination of both methods, the calculation of the manifold and the steps-to-fall method.

The area of the basin of attraction as a measure for robustness is shown in Fig. 5(b). Two maxima of the area can be found: the first maximum at $\widetilde{k} \approx 15$ for symmetric walking patterns, and the second at $\widetilde{k} \approx 11$ for asymmetric walking. With increasing leg stiffness the area decreases. This is due to the fact that with increasing leg stiffness the angle of attack is shifted toward larger angles. Hence, the touch down height $y_{\mathrm{TD}}(\alpha_0)$ increases and limits the basin of attraction. Furthermore, at higher stiffness the basin of attraction is more limited with respect to initial velocity angles θ_0 compared to lower leg stiffness. At the transcritical bifurcation the area is minimal. In the majority of cases in symmetric walking, with increasing area of the basin of attraction, the corresponding Floquet multiplier converges towards one.

IV. Robot experiment

So far, walking was investigated using the bipedal spring-mass model. In this section we will present preliminary walking experiments done with the bipedal robot PogoWalker (Fig. 6(a)), which has prismatic legs with a rest length of $0.58\,\mathrm{m}$. The leg force is generated by springs with an overall leg stiffness of $\widetilde{k} \approx 20$. The PogoWalker weighs $4.1\,\mathrm{kg}$ and its mass is concentrated at the upper body. During the experiments about 10% of the robots weight was suspended by elastic cords to prevent from falling. In each

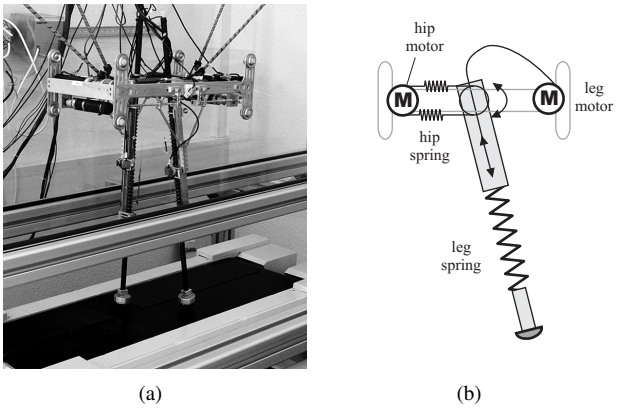

Fig. 6. The bipedal PogoWalker in (a) with compliant telescoping legs walking on the instrumented treadmill. The schematic in (b) illustrates the motor configuration for one leg.

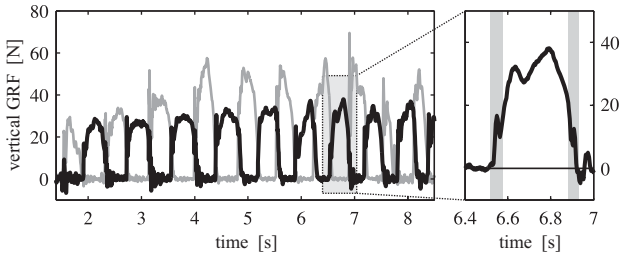

Fig. 7. Vertical ground reaction forces (GRF) of PogoWalker measured with treadmill sensors. The forces are separated for both legs and were recorded with 200 Hz.

leg two motors are implemented: one motor actuates the hip, elastically coupled with belts and another shortens the legs during swing phase using a flexible cable.

The control is separated into three phases. During stance phase, the leg is retracted with a speed matching the treadmill speed. After lift off, the leg is actively shortened and protracted until a leg angle of $\alpha_0 \approx 70\,\mathrm{deg}$ is reached. The elastic coupling of the hip motor generates a slightly underdamped system. Small deviations of the leg angle α_0 from the desired value occur within small fractions of the step time. In the last phase, the leg waits in the mentioned leg position until touch down occurs, which is detected by foot force sensors.

The PogoWalker moved on an instrumented treadmill that is purpose-built for robot experiments (Tecmachine, Andrezieux Boutheon, France). The treadmill has integrated force sensors (Kistler, Winterthur, Switzerland) to measure three dimensional ground reaction forces of both legs separately. Fig. 7 shows vertical forces of a walking experiment at a treadmill speed of $0.46\,\mathrm{m/s}$. After a few seconds the robot mechanically adapts to the motion and shows first double humped ground reaction forces. The selected force pattern is related in shape to the asymmetric pattern E in Fig. 3.

At initial stance phase the forces have a peak that is in most cases not larger than the active peak during single support. Both legs generate noticeably different ground reaction forces, caused by an asymmetry in the robot construction.

V. DISCUSSION

The objectives of this study were (1) the identification of periodic walking patterns, (2) the extraction of a leg stiffness that provides stable and robust walking, and (3) a verification of the advantages of compliant legs on a robot experiment. In this section we discuss primary findings, starting with the leg stiffness for stable and robust bipedal walking.

There exists a range of $\widetilde{k} = [10, 20]$ where the model shows both, self-stability and comparatively large robustness against perturbations. Moreover, as the range of angles of attack providing stable walking is large, there is no need for precise leg adjustment in preparation for touch down. This enables a relaxed leg placement control for continuing walking as demonstrated with PogoWalker.

The PogoWalker's leg stiffness is located at the upper limit of the indicated stiffness range. However, this stiffness might be a compromise between robustness and energy efficiency. The lower the stiffness, the more the leg will be compressed and more energy might be dissipated [14]. The extreme case of bipedal walking are passive dynamic walkers with almost infinite leg stiffness, showing high energy efficiency but low robustness. This can be approximated from Fig. 5(b), as the basin of attraction clearly decreases with increasing stiffness.

The size of the basin of attraction is not directly related to the orbital stability, expressed by the maximum Floquet multiplier [15]. A stable walking pattern with a large basin of attraction is often less orbitally stable. Although, it takes many walking steps to reduce a small perturbation, even large perturbations are manageable as it was shown for passive dynamic walking on irregular surfaces [15].

The bipedal spring-mass model predicts that walking with compliant legs can be much faster than the speed at which humans naturally change from walking to running ($\approx 2\,\mathrm{m/s}$) [16]. In these fast walking patterns (related to pattern B in Fig. 3) Floquet multipliers indicate highly unstable behavior with values clearly exceeding the stability limitation of $\max|\lambda| = 1$. We assume that such gaits can be stabilized by combinations of swing-leg strategies, i.e. swing-leg retraction, and adaptation of leg stiffness and leg length [10].

Another drawback of fast walking patterns are very short swing durations, as can be estimated from pattern B in Fig. 3. This seems not feasible for robots with heavy legs. The velocity limit of more natural walking (related to pattern A) is found at $1.4\,\mathrm{m/s}$, which is a medium walking speed for humans. We assume that the linear force-length relationship of the investigated legs limits this speed and that this speed range could be enhanced by non-linear leg functions. A decreasing force-length relationship owing to leg segmentation improves stability in running at moderate speeds [17] and it remains for further investigations to prove whether it enhances walking too.

The walking patterns identified in the low dimensional bipedal spring-mass model are a basis for legged systems with more parameters and state space variables. For example, the symmetric walking patterns are completely inherited in a simulation model with a distributed upper body, that was established for testing a novel hip control to stabilize the trunk [18]. In a forthcoming study, we will prove the technical feasibility of this hip control in the PogoWalker.

In contrast to the PogoWalker, our model doesn't have leg mass. However, this simplified model is a good template for describing complex walking systems [4]. Extending the model with leg masses would require further model extensions, namely energy recovery mechanisms to compensate impact losses, and a distributed body to counteract the hip torques during swing phase. We expect that the most prominent system properties are the representation of impacts and the limitation of the solution space to walking patterns with reasonable swing times. The bipedal spring-mass model may help to reveal new system features.

REFERENCES

[1] S. H. Collins, A. Ruina, R. L. Tedrake, and M. Wisse, "Efficient bipedal robots based on passive-dynamic walking," *Science*, vol. 307, no. 5712, pp. 1082–1085, 2005.

[2] D. G. E. Hobbelen and M. Wisse, "A disturbance rejection measure for limit cycle walkers: The gait sensitivity norm," *IEEE Trans. Robot.*, vol. 23, no. 6, pp. 1213–1224, 2007.

[3] C. R. Lee and C. T. Farley, "Determinants of the center of mass trajectory in human walking and running," *J. Exp. Biol.*, vol. 201, no. 21, pp. 2935–2944, 1998.

[4] H. Geyer, A. Seyfarth, and R. Blickhan, "Compliant leg behaviour explains basic dynamics of walking and running," *Proc. R. Soc. B*, vol. 273, no. 1603, pp. 2861–2867, 2006.

[5] A. Seyfarth, K. T. Kalveram, and H. Geyer, "Simulating muscle-reflex dynamics in a simple hopping robot," in *Autonome Mobile Systeme 2007*. Kaiserslautern, Germany: Springer, 2007, pp. 294–300.

[6] M. d. Lasa and M. Buehler, "Dynamic compliant quadruped walking," in *Proc. IEEE Int. Conf. Robotics and Automation*, Seoul, Korea, 2001, pp. 3153–3158.

[7] B. Verrelst, "A dynamic walking biped actuated by pleated pneumatic artificial muscles: Basic concepts and control issues," Ph.D. thesis, Vrije Universiteit Brussel, 2005.

[8] F. Iida, J. Rummel, and A. Seyfarth, "Bipedal walking and running with compliant legs," in *Proc. IEEE Int. Conf. Robotics and Automation*, Roma, Italy, 2007, pp. 3970–3975.

[9] A. Seyfarth, F. Iida, R. Tausch, M. Stelzer, O. von Stryk, and A. Karguth, "Towards bipedal jogging as a natural result of optimizing walking speed for passively compliant three-segmented legs," *Int. J. Robot. Res.*, vol. 28, no. 2, pp. 257–265, 2009.

[10] Y. Blum, S. W. Lipfert, J. Rummel, and A. Seyfarth, "Swing leg control in human running," *J. R. Soc. Interface*, (under review).

[11] J. Guckenheimer and P. Holmes, *Nonlinear Oscillations, Dynamical Systems, and Bifurcations of Vector Fields*, ser. Applied Mathematical Sciences. New York: Springer, 1983, vol. 42.

[12] T. S. Parker and L. O. Chua, *Practical numerical algorithms for chaotic systems*. New York: Springer, 1989, 66797.

[13] M. Srinivasan and P. Holmes, "How well can spring-mass-like telescoping leg models fit multi-pedal sagittal-plane locomotion data?" *J. Theor. Biol.*, vol. 255, no. 1, pp. 1–7, 2008.

[14] M. Srinivasan and A. Ruina, "Computer optimization of a minimal biped model discovers walking and running," *Nature*, vol. 439, no. 7072, pp. 72–75, 2006.

[15] J. L.-S. Su and J. B. Dingwell, "Dynamic stability of passive dynamic walking on an irregular surface," *J. Biomech. Eng.*, vol. 129, no. 6, pp. 802–810, 2007.

[16] A. Hreljac, "Preferred and energetically optimal gait transition speeds in human locomotion," *Med. Sci. Sports Exerc.*, vol. 25, no. 10, pp. 1158–1162, 1993.

[17] J. Rummel and A. Seyfarth, "Stable running with segmented legs," *Int. J. Robot. Res.*, vol. 27, no. 8, pp. 919–935, 2008.

[18] H.-M. Maus, J. Rummel, and A. Seyfarth, "Stable upright walking and running using a simple pendulum based control scheme," in *Advances in Mobile Robotics: Proc. 11th Int. Conf. Climbing and Walking Robots*. Coimbra, Portugal: World Scientific, 2008, pp. 623–629.